JOURNAL OF ELECTROMAGNETIC ENGINEERING AND SCIENCE, VOL. 19, NO. 3, 188~196, JUL. 2019

https://doi.org/10.26866/jees.2019.19.3.188
ISSN 2671-7263 (Online) · ISSN 2671-7255 (Print)

A Compact Rx Antenna Integration for 3D Direction-Finding Passive Radar

Hojoo Lee[1] · Jaesik Kim[2] · Jaehoon Choi[1,*]

Abstract

A compact receiving (Rx) antenna integration for 3D direction-finding passive radar is proposed. The proposed antenna integration consists of two Yagi antennas and two waveguide slot antennas. The antennas are mounted on four sides of a parallelepiped polycarbonate module with the same type of antennas facing each other on the opposite sides of the module. The antenna is designed for a direction-finding radar system as an Rx terminal on an avionic vehicle with a separate Tx base station on the ground. The proposed antenna integration demonstrates a maximum return loss of 9.6 dB (voltage standing wave ratio 2:1) ranging from 9.7 to 10.2 GHz in the X band and has suitable radiation patterns for direction-finding system in both the *xz* and *yz* planes. In addition, the proposed antenna integration has the compact size and light gross weight of 37 mm × 46 mm × 50 mm and 97 g, respectively, making it suitable for application in an avionic system.

Key Words: Direction-Finding, Radar, Waveguide Slot Antenna, Yagi Antenna.

I. Introduction

With the rapid development of commercial and military avionic radar systems, interest in antenna design technology for guidance and control systems for avionic vehicles has increased explosively during the past few years. To meet the performance requirements of the antennas mounted on an object for direction-finding, many studies have been conducted [1–6]. To reduce power consumption, the antenna usually operates in passive Rx mode, with an additional Tx base station on the ground [7], as shown in Fig. 1. The Tx station first transmits a signal to the target in the air. When the reflected signal from the target hits the Rx antenna, the front-end receiver module deduces the amplitude of it as DC voltage [8, 9]. After processing and computing that voltage value, the direction of the incoming signal can be found by analyzing the differential amplitude of the volt-

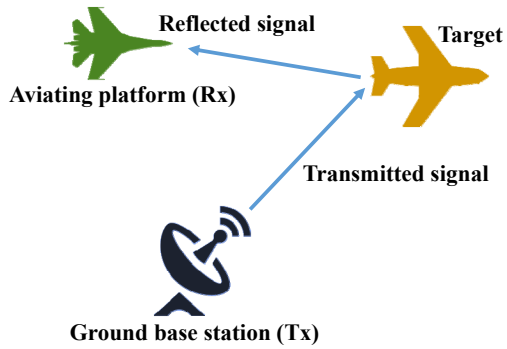

Fig. 1. Operating principal of the application.

Manuscript received December 05, 2018 ; Revised March 27, 2019 ; Accepted May 17, 2019. (ID No. 20181205-085J)
[1]Department of Electronics and Communications Engineering, Hanyang University, Seoul, Korea.
[2]Agency for Defense Development, Daejeon, Korea.
[*]Corresponding Author: Jaehoon Choi (e-mail: choijh@hanyang.ac.kr)

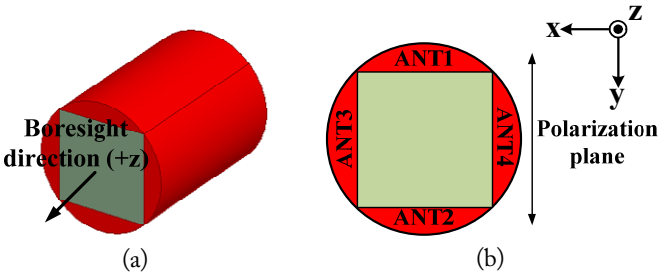

Fig. 2. Four antennas mounted on a paralleled piped module for direction-finding application: (a) perspective view and (b) front view.

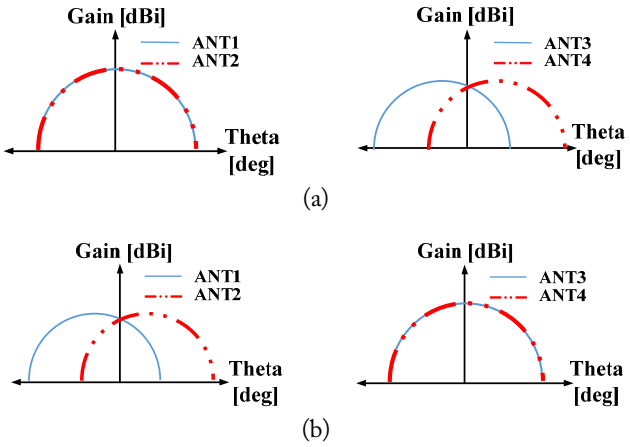

Fig. 3. A brief example of ideally suitable radiation patterns on *xz* plane (a) and *yz* plane (b).

age measured from each Rx channel. Thus in the industrial field, multi-channel Rx antenna integrations are generally used [10]. Each antenna is mounted on four faces of a parallelepiped antenna module on an avionic vehicle as shown in Fig. 2. When using the amplitude comparison scheme for direction-finding, ambiguity of the gain amplitude can become an issue that affects the accuracy of the system [11]. To eliminate that ambiguity in a four-channel direction-finding system, the radiation patterns of the four antennas in Fig. 2 should be similar to the patterns shown in Fig. 3 [12]. In the ideal of that case, the gain difference between ANT1–ANT2 and ANT3–ANT4 in *xz* and *yz* planes can be graphically deduced as the plots given in Fig. 4. To satisfy all those properties, we here propose a compact and light-weight Rx antenna integration suitable for a 3D direction-finding radar system.

II. Design of Single Antenna Elements

With reference to the radiation patterns in Fig. 3, four antennas need to be chosen to generate the required beam patterns. However, because the Tx antenna of a ground base station system usually has a sharp beam with linear polarization [13, 14] (e.g., dipole or patch array), the linearly polarized planes of the

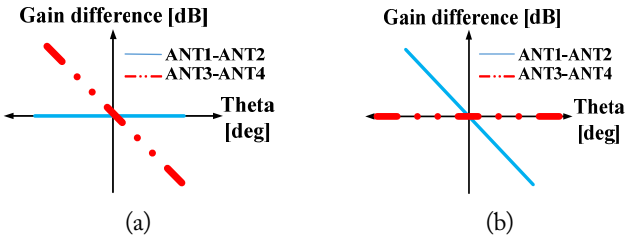

Fig. 4. A brief example of ideal gain difference between ANT1–ANT2 and ANT3–ANT4 in (a) *xz* plane (b) *yz* plane.

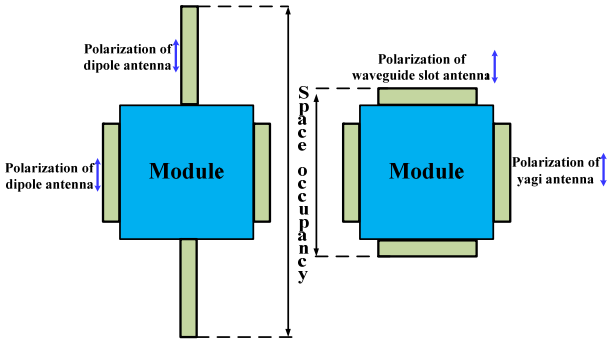

Fig. 5. Comparison of space occupancy between two types of antenna integration using (a) four identical antennas and (b) two types of antenna pairs with polarization orthogonal to each other.

four Rx antennas must coincide with one another to receive the reflected signal from the target. One way to obtain that property is to use four identical antennas, such as a dipole antenna on each side of the platform, as shown in Fig. 5(a). However, that configuration requires a significant amount of space for the antennas. Therefore, we propose two Yagi antennas and two waveguide slot antennas for ANT1–ANT2 and ANT3–ANT4 in Fig. 2, respectively, as shown in Fig. 5(b), which requires much less space.

1. Microstrip Yagi Antenna

The single element for a microstrip Yagi antenna is illustrated in Fig. 6. The antenna consists of an SMA connector, dipole element, rear reflector, front driver, polycarbonate (PC) spacer, bottom reflector, and two PC bolt screws. Parameters of the antenna were calculated using the basic properties of a general Yagi antenna [15], as shown in Table 1, and then fine-tuning them using HFSS software (version 2016.2, Ansys Corporation, Pittsburgh, PA, USA). The simulated return loss of the antenna is shown in Fig. 7. The bandwidth of the antenna to achieve voltage standing wave ratio (VSWR) 2:1 is 9.25–11.8 GHz. As a conventional Yagi antenna, the antenna has a directive and nearly symmetric radiation pattern in the *xz* plane [16], as shown in Fig. 8. On the other hand, the antenna exhibits a tilted beam from the +z to +y direction at 50°, as shown in Fig. 8,

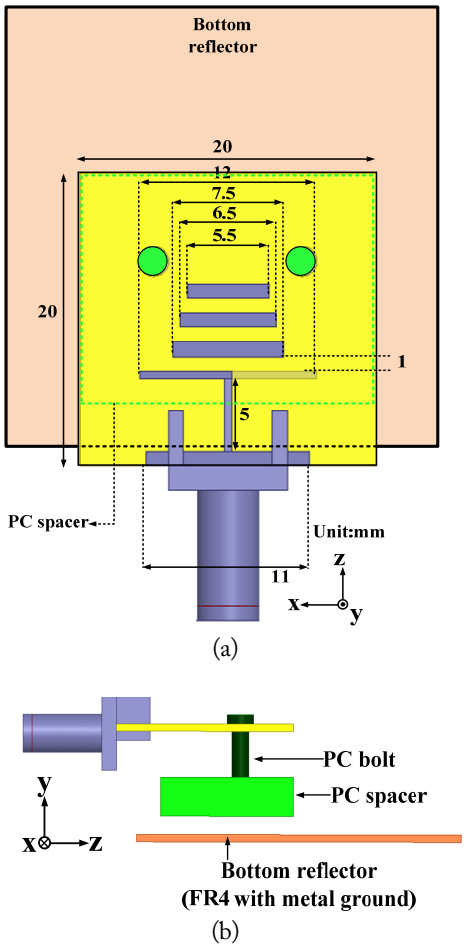

Fig. 6. Geometry of the proposed Yagi antenna element: (a) top view and (b) side view.

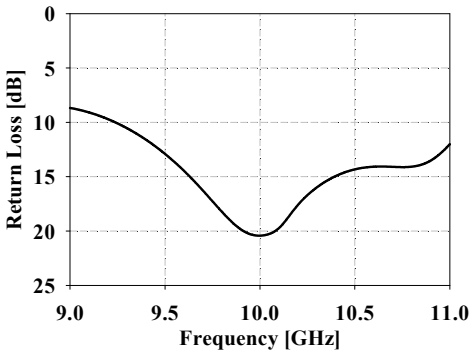

Fig. 7. Simulated return loss of the Yagi antenna element.

due to the bottom reflector made of FR4 substrate with a full metal pattern on its upper side. In addition, the antenna is linearly polarized in the *xz*-plane according to the nature of a dipole antenna [17].

2. Waveguide Slot Antenna

The single element of a waveguide slot antenna is designed as shown in Fig. 9. The resonant frequency is determined by the half-wavelength (λ/2) central slot on the top of the waveguide.

Table 1. Theoretical values for parameter of Yagi antenna

Parameter	Theoretical value
Distance	
Reflector to dipole	0.2-0.35λ
Director to director	0.2-0.35λ
Width	
Dipole	0.015-0.025λ
Director	0.015-0.025λ
Length	
Dipole	0.45-0.49λ
Director	0.4-0.45λ
Reflector	≈0.5λ

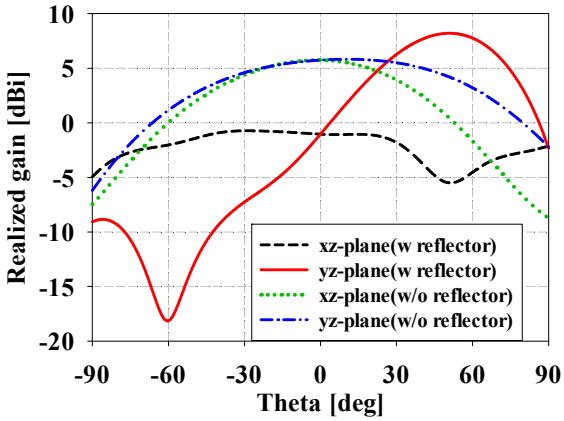

Fig. 8. Simulated radiation pattern of the Yagi antenna element at 10 GHz with and without bottom reflector.

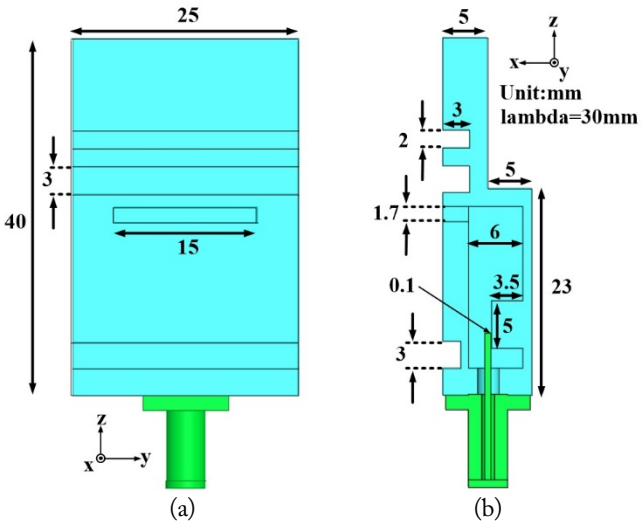

Fig. 9. Geometry of the proposed waveguide slot antenna element: (a) top view and (b) cross-sectional side view.

Impedance matching was achieved by placing a conducting metal block inside the waveguide and adjusting the gap between the feeder pin and the block. The simulated result shows that the bandwidth of the antenna to achieve VSWR 2:1 is 9.85–10.23 GHz, as shown in Fig. 10. Unlike conventional waveguide slot antennas [18–20], the waveguide slot antenna in this

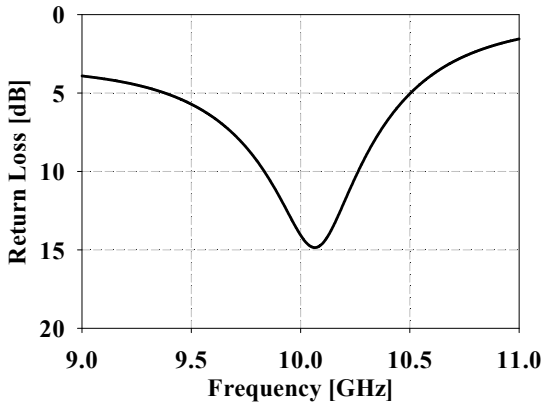

Fig. 10. Simulated return loss of the waveguide slot antenna element.

paper has three corrugation grooves on the top wall of the waveguide. The one in the rear is for suppressing the surface wave toward –z direction, and the two in the front induce more surface wave toward the +z direction. The former is placed λ/2 away from the slot and the latter are located close to the slot to obtain the tilted main beam [21–23]. Fig. 11 illustrates the effect of each corrugation on the main beam direction of the antenna in the *xz* plane. As a final optimized result, the main beam of the waveguide slot antenna in the *xz* plane is tilted 45° from the +x direction to the +z direction while being symmetric in the *yz* plane, as shown in Fig. 12. In addition, the antenna is linearly polarized in the *xz* plane according to the nature of a waveguide slot antenna [17].

III. Antenna Integration Design

As illustrated in the previous section, the antenna integration consists of two Yagi antennas (Y1 and Y2) and two waveguide slot antennas (B1 and B2) mounted on each side of the plastic module, as shown in Fig. 13. Considering the position of the mounted antennas, the linearly polarized plane of the four antennas is identical (i.e., coincides with the *xz* plane) due to the

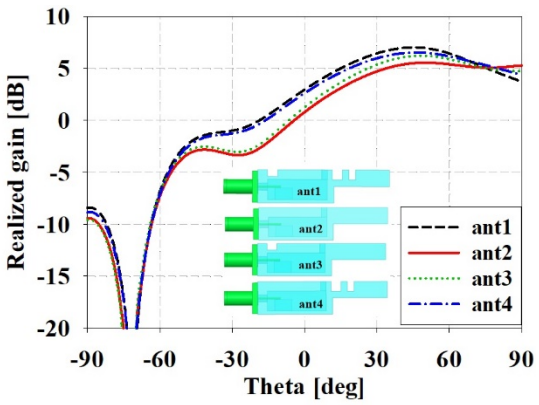

Fig. 11. The effect of corrugation grooves on the radiation pattern of the antenna in *xz* plane.

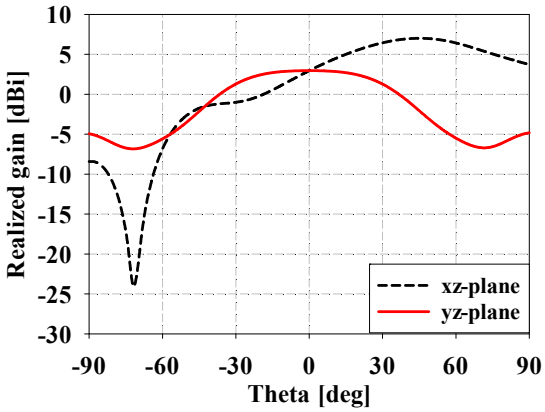

Fig. 12. Simulated radiation pattern of the waveguide slot antenna element in both *xz* and *yz* planes at 10 GHz.

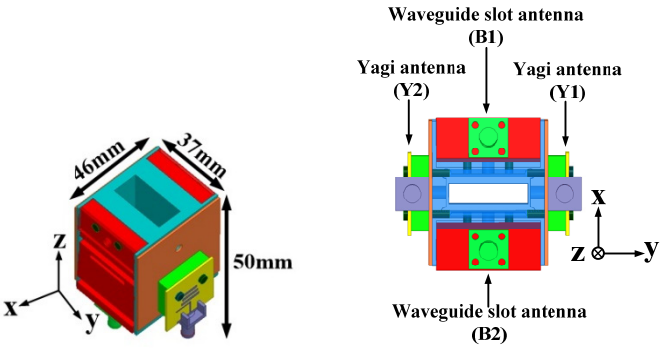

Fig. 13. Geometry of the proposed antenna integration: (a) perspective view and (b) rear view.

polarization characteristics of the antenna types. The module for mounting the integrated antennas is made of PC ($\varepsilon_r = 2.8$), which is economical, easily machinable, and lightweight. The simulated return loss characteristics of the antenna mounted on the module are shown in Fig. 14. All four antennas satisfy the maximum return loss level of 9.6 dB (i.e., VSWR 2:1) from 9.85 GHz to 10.15 GHz. Fig. 15 briefly illustrates the E-field distributions of both antennas mounted on the module to verify the origination of the tilted main beams in both the *xz* and *yz*

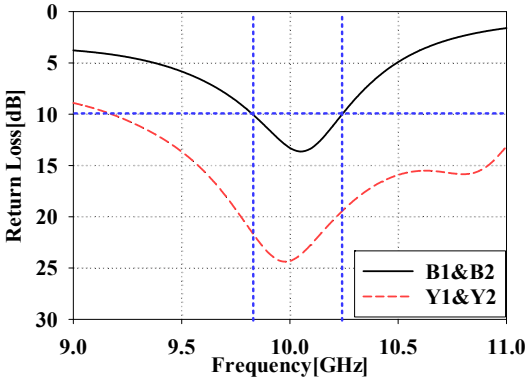

Fig. 14. Simulated return loss of the proposed antennas.

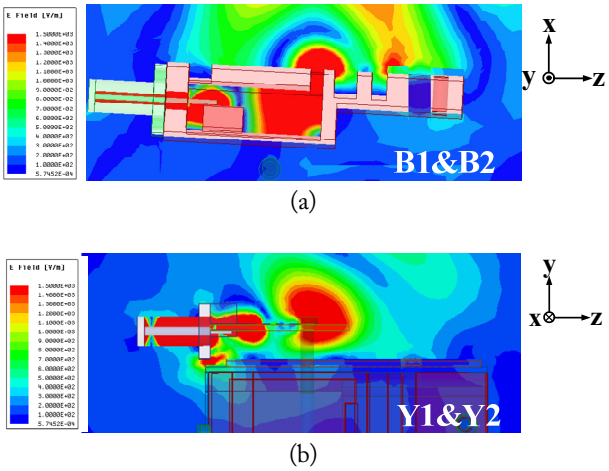

Fig. 15. E-field distributions of two antenna types at 10 GHz: (a) waveguide slot antenna in *xz* plane and (b) Yagi antenna in *yz* plane.

planes. Compared with the proposed Yagi antenna in the *yz* plane, the waveguide slot antenna has a broader radiation pattern in the *xz* plane due to the nature of the antenna mechanism. Therefore, to obtain a steeper gradient—i.e., larger value of (dBi/theta degree)—for the gain plot in the *xz* plane, both waveguide slot antennas are rotated about 3° toward the z-axis, which makes the radiation pattern similar to that in Fig. 3. As shown in Fig. 16, the gradient of the gain decrement versus theta becomes steeper in general as the antenna is rotated but starts to flatten from 4°. Fig. 17 illustrates the optimized result for simulated radiation patterns of the proposed antenna integration at 10 GHz in the *xz* and *yz* planes. As shown in the figure, the radiation patterns of the B1 and B2 are identical in the *yz* plane and symmetric in the *xz* plane. On the other hand, the radiation patterns of Y1 and Y2 are identical in the *xz* plane and symmetric in the *yz* plane. In addition, the maximum gains of the B-type antennas in *xz* plane and the Y-type antennas in *yz* plane are 7.5 dBi and 8.1 dBi, respectively.

To analyze the suitability of the radiation pattern illustrated in Fig. 3, we conducted a graphical manipulation. The plots in

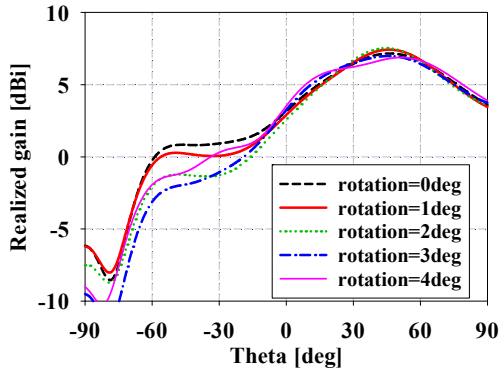

Fig. 16. Effect of the rotation of the waveguide slot antenna on the gradient of the gain versus theta in *xz* plane.

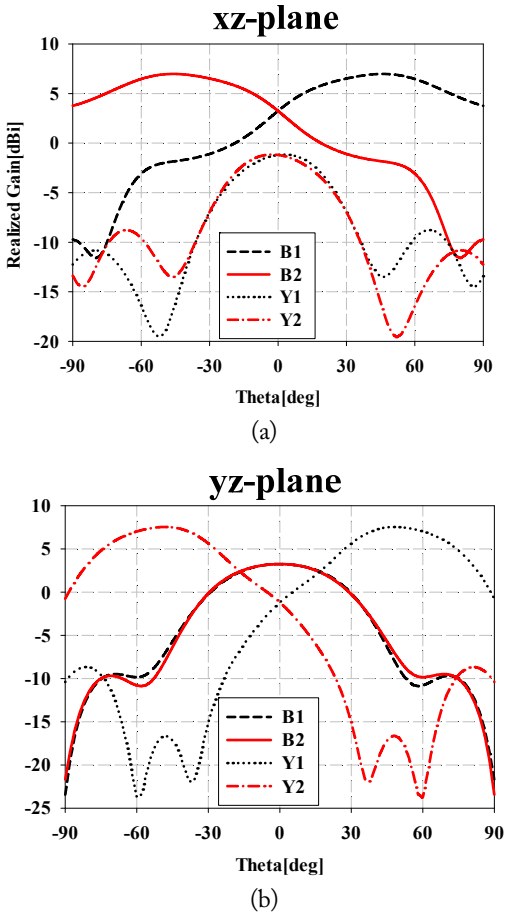

Fig. 17. Simulated radiation patterns of the proposed antenna at 10 GHz: (a) *xz* plane and (b) *yz* plane.

Fig. 18 indicate the gain difference between the antennas with identical types in the *xz* and *yz* planes at 10 GHz. The gradient of the gain difference plots between B1 and B2 in the *xz* plane and Y1 and Y2 in the *yz* plane are steep, whereas that between B1 and B2 in the *yz* plane and Y1 and Y2 in the *xz* plane are relatively flat. Thus, the antenna integration generally satisfies the property explained in Fig. 4. However, there is a certain range within which its performance deteriorates (e.g., $|\text{theta}| > 40°$ in both the *xz* and *yz* plane). Outside that range, the radiation patterns of the proposed antenna integration offer good performance for direction-finding application. On the other hand, the slope of gain differences of Y1 and Y2 in the *yz* plane and B1 and B2 in the *yz* plane are not identical to each other. However, this can be overcame by employing calibration factor to the gain difference slope at the signal processing stage in order to eliminate possible error of the direction finding system.

IV. Experimental Results

1. Fabrication of the Proposed Antenna

Because the proposed antenna integration combines four antennas onto a plastic assemblage module, three mechanical pro-

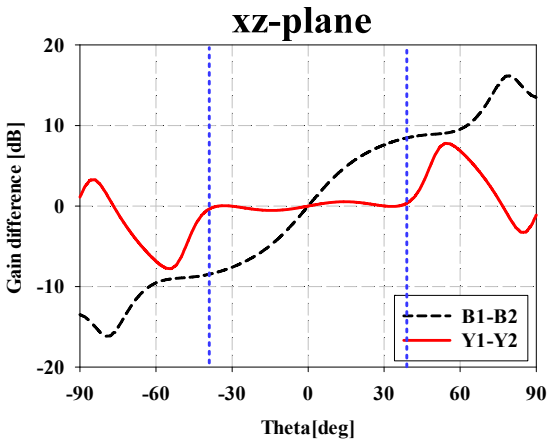

(a)

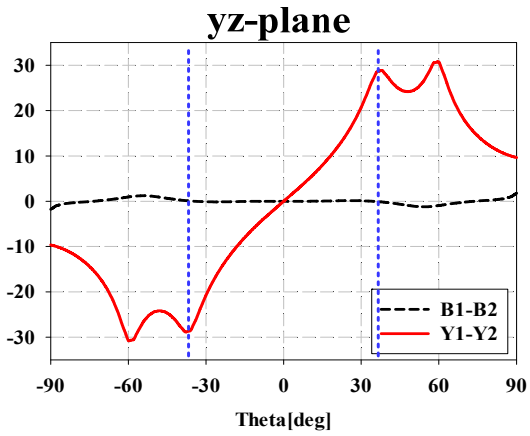

(b)

Fig. 18. Gain difference between B1–B2 and Y1–Y2 at 10 GHz vs. theta: (a) *xz* plane and (b) *yz* plane.

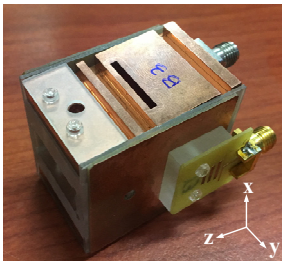

(a)

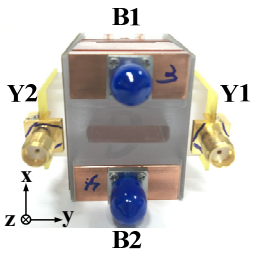

(b)

Fig. 19. Fabricated antenna integration: (a) perspective view and (b) rear view.

cessing techniques were used to fabricate the whole structure. First, computer numerical control (CNC) machining was used to manufacture the PC module and spacer. PC was used because it is inexpensive, easily machinable, and has a relatively high tolerance to heat and impact [24]. Second, an etching process was used to fabricate the Yagi antenna and FR4 reflector. For the waveguide slot antennas, electroforming was applied because the bent inner space is difficult to realize using CNC machining [25]. To minimize unexpected degradations in performance, all the bolts used to fasten the subparts were made of PC. Fig. 19 illustrates the finalized antenna integration. The total dimensions of the proposed antenna integration are 37 mm × 46 mm × 50 mm and its gross weight is 97 g. Therefore, the proposed antenna integration is both compact and light, which are great features for being mounted onto an avionic vehicle system.

2. Measured Results

The return loss and radiation pattern of the assembled anten-

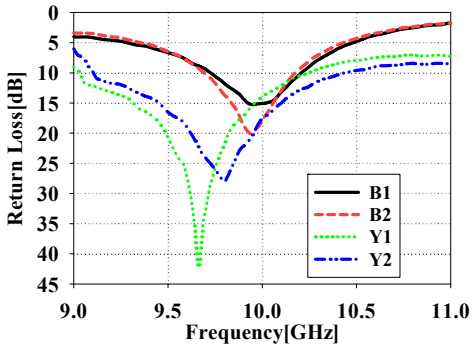

Fig. 20. Measured return loss of the proposed antennas.

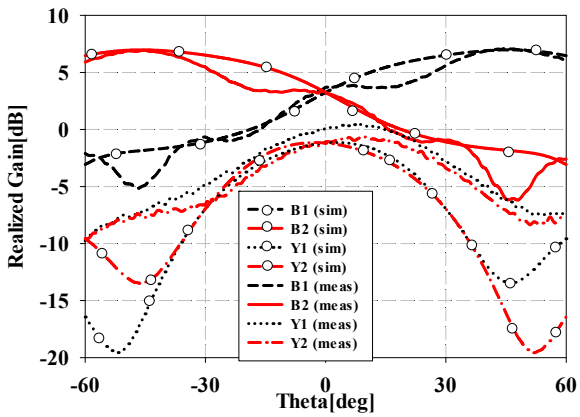

(a)

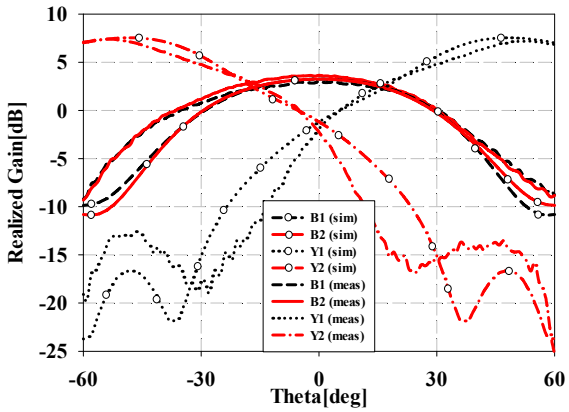

(b)

Fig. 21. Simulated and measured radiation patterns of the proposed antenna at 10 GHz: (a) *xz* plane and (b) *yz* plane.

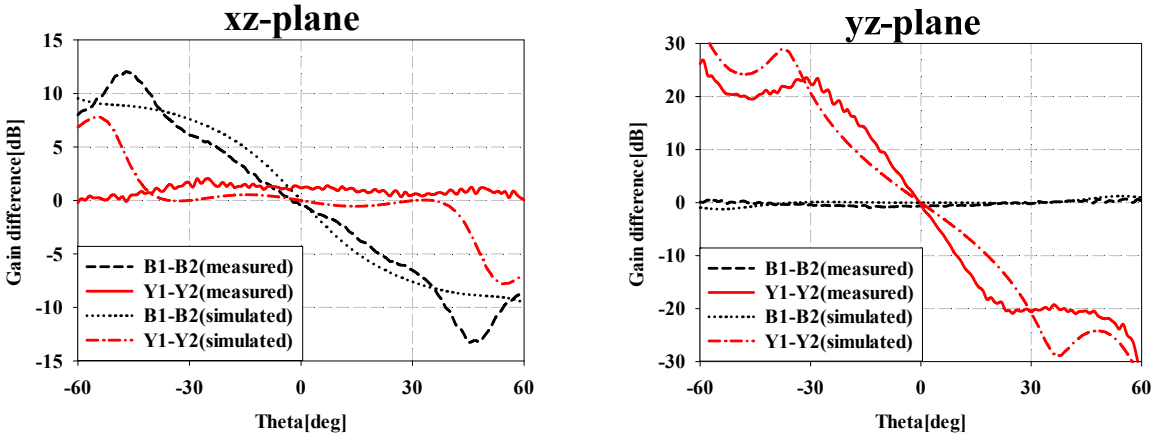

(a) (b)

Fig. 22. Comparison between simulated and measured gain difference between B1–B2 and Y1–Y2 at 10 GHz vs. theta: (a) *xz* plane and (b) *yz* plane.

na integration were experimentally verified. Fig. 20 shows the measured return loss characteristics of the proposed antennas. As shown in Fig. 20, the 9.6 dB return loss bandwidths are from 9.7 to 10.2 GHz for B1–B2 and from 9.1 to 10.2 GHz for Y1–Y2. Fig. 21 shows the measured radiation patterns of the proposed antenna. As shown Fig. 21, the radiation patterns for B1–B2 are symmetric and mostly identical in the *xz* and *yz* planes, respectively. On the other hand, the radiation patterns of Y1–Y2 are mostly identical and symmetric in the *xz* and *yz* planes, respectively as illustrated in Fig. 22. By evaluating the measured gain difference between the two antennas of the same type, the plot of B1–B2 (i.e., gain difference between B1 and B2 vs. theta) and Y1–Y2 (i.e., gain difference between Y1 and Y2 vs. theta) in both the *yz* and *xz* planes are similar to those in Fig. 4. In addition, the integrity of the proposed design is verified because the simulated and measured results agree well with each other. Therefore, the proposed antenna integration is suitable for direction-finding. Furthermore, based on the result shown in Fig. 22, the ranges of the detection angle (theta) for direction-finding in the *yz* and *xz* planes are excellent: $|\text{theta}| < 30°$ and $|\text{theta}| < 45°$, respectively. In addition, as shown in Fig. 21, the simulated and measured results agree well with each other except for a small range of angles, verifying the integrity of the antenna integration design. The overall performance of the proposed antenna integration is summarized in Table 2.

V. Conclusion

In this paper, we have proposed a compact, lightweight Rx antenna integration suitable for 3D direction-finding radar. The proposed antenna integration exhibits a return loss value under 9.6 dB in the frequency band range from 9.7 to 10.2 GHz. The radiation patterns of the proposed antenna in both the *yz* and *xz* planes are generally suitable for a direction-finding system. In addition, the proposed antenna integration is both compact and light. Therefore, when combined with an appropriate receiver module for extracting DC voltage, it is a good antenna candidate for a direction-finding system for an avionic object.

This research was supported by the Agency for Defense Development, Korea.

Table 2. Summary of the performance of the proposed antenna integration

	B1	B2	Y1	Y2
VSWR 2:1 bandwidth (GHz)	9.8-10.3	9.7-10.2	9.1-10.2	9.2-10.4
Main beam (dBi@deg)	7.1@43	7.0@-42	7.5@50	7.4@-52
Half power beamwidth (deg)				
xz-plane	59	61	49	50
yz-plane	65	63	57	55
Gradient of gain difference (dB/deg)				
xz-plane	Average 0.27 (relatively steep)		Average 0.05 (relatively flat)	
yz-plane	Average 0.02 (relatively flat)		Average 0.77 (relatively steep)	

REFERENCES

[1] E. Ferrar and T. Parks, "Direction finding with an array of antennas having diverse polarizations," *IEEE Transactions on Antennas and Propagation*, vol. 31, no. 2, pp. 231-236, 1983.

[2] J. Yeo and J. I. Lee, "Miniaturized LPDA antenna for portable direction finding applications," *ETRI Journal*, vol. 34, no. 1, pp. 118-121, 2012.

[3] J. H. Choi, C. S. Park, S. P. Nah, and W. Jang, "A multichannel correlative vector direction finding system using active dipole antenna array for mobile direction finding applications," *Journal of Electromagnetic Engineering and Science*, vol. 7, no. 4, pp. 161-168, 2007.

[4] A. Farina and H. Kuschel, "Guest editorial special issue on passive radar (Part I)," *IEEE Aerospace and Electronic Systems Magazine*, vol. 27, no. 10, pp. 5-5, 2012.

[5] H. D. Griffiths and C. J. Baker, "Passive coherent location radar systems. Part 1: Performance prediction," *IEE Proceedings-Radar, Sonar and Navigation*, vol. 152, no. 3, pp. 153-159, 2005.

[6] C. J. Baker, H. D. Griffiths, and I. Papoutsis, "Passive coherent location radar systems. Part 2: Waveform properties," *IEE Proceedings-Radar, Sonar and Navigation*, vol. 152, no. 3, pp. 160-168, 2005.

[7] P. Knott, "Design of a printed dipole antenna array for a passive radar system," *International Journal of Antennas and Propagation*, vol. 2013, article ID. 179296, 2013.

[8] H. Peng, Z. Yang, and T. Yang, "Design and implementation of a practical direction finding receiver," *Progress In Electromagnetics Research Letters*, vo. 32, pp. 157-167, 2012.

[9] N. D. Au and C. Seo, "A novel design of an RF-DC converter for a low–input power receiver," *Journal of Electromagnetic Engineering and Science*, vol. 17, no. 4, pp. 191-196, 2017.

[10] N. M. Mitrovic and M. M. Ponjavic, "Multichannel 2-D direction finding based on differential amplitude detection," *IEEE Sensors Journal*, vol. 15, no. 9, pp. 5064-5070, 2015.

[11] Q. Zhu, S. Yang, R. Yao, and Z. Nie, "Direction finding using multiple sum and difference patterns in 4D antenna arrays," *International Journal of Antennas and Propagation*, vol. 2014, article no. 392895, 2014.

[12] R. B. Dybdal, "Monopulse resolution of interferometric ambiguities," *IEEE Transactions on Aerospace and Electronic Systems*, vol. 22, no. 2, pp. 177-183, 1986.

[13] H. S. Setiadji, F. Y. Zulkifli, and E. T. Rahardjo, "Radiation characteristics of microstrip array antenna for x-band radar application," in *Proceedings of 2016 Progress in Electromagnetic Research Symposium (PIERS)*, Shanghai, China, 2016, pp. 3992-3995.

[14] I. Slomian, K. Wincza, and S. Gruszczynski, "Low-cost broadband microstrip antenna array for 24 GHz FMCW radar applications," *International Journal of RF and Microwave Computer-Aided Engineering*, vol. 23, no. 4, pp. 499-506, 2013.

[15] C. Balanis, *Antenna Theory*, 3rd ed. Hoboken, NJ: John Wiley & Sons, 2005.

[16] V. Bankey and N. A. Kumar, "Design of a Yagi-Uda antenna with gain and bandwidth enhancement for Wi-Fi and Wi-Max applications," *International Journal of Antennas*, vol. 2, no. 1, pp. 1-14, 2016.

[17] Y. T. Lo and S. W. Lee, *Antenna Handbook*. New York, NY: Van Nostrand Reinhold, 1993.

[18] S. Trinh-Van, S. C. Song, S. H. Seo, and K. C. Hwang, "Waveguide slot array antenna with a hybrid-phase feed for grating lobe reduction," *International Journal of Antennas and Propagation*, vol. 2016, article ID. 4825924, 2016.

[19] Q. Fang, L. Song, and M. Jin, "Design and simulation of a waveguide slot antenna," in *Proceedings of 2012 5th Global Symposium on Millimeter-Waves*, Harbin, China, 2012, pp. 131-134.

[20] S. Pandit, A. Mohan, and P. Ray, "A low-profile high-gain substrate-integrated waveguide-slot antenna with suppressed cross polarization using metamaterial," *IEEE Antennas and Wireless Propagation Letters*, vol. 16, pp. 1614-1617, 2017.

[21] Y. Jin, H. Lee, D. Woo, and J. Choi, "Low-profile tilted-beam waveguide slot antenna using corrugations for UAV applications," *Microwave and Optical Technology Letters*, vol. 60, no. 2, pp. 341-347, 2018.

[22] M. Beruete, I. Campillo, J. S. Dolado, J. E. Rodrguez-Seco, E. Perea, F. Falcone, and M. Sorolla, "Very low profile and dielectric loaded feeder antenna," *IEEE Antennas and Wireless Propagation Letters*, vol. 6, pp. 544-548, 2007.

[23] M. Beruete, I. Campillo, J. S. Dolado, J. E. Rodriguez-Seco, E. Perea, F. Falcone, and M. Sorolla, "Very low-profile" Bull's Eye" feeder antenna," *IEEE Antennas and Wireless Propagation Letters*, vol. 4, pp. 365-368, 2005.

[24] J. G. Chen, T. Zhang, J. S. Zhu, X. Y. Zhang, J. L. Zhou, J. F. Fan, and G. H. Hu, "Low-loss planar optical waveguides fabricated from polycarbonate," *Polymer Engineering & Science*, vol. 49, no. 10, pp. 2015-2019, 2009.

[25] J. A. McGeough, M. C. Leu, K. P. Rajurkar, A. K. M. De Silva, and Q. Liu, "Electroforming process and application to micro/macro manufacturing," *CIRP Annals*, vol. 50, no. 2, pp. 499-514, 2001.

Hojoo Lee

received his B.S. and M.S. degrees in Electronics and Computer Engineering from Hanyang University in Seoul, Korea, in 2010 and 2015. He is currently working toward a Ph.D. degree in the Department of Electronics and Computer Engineering at Hanyang University in Seoul, Korea. His current research interest focuses on various RF devices, waveguide components and antenna designs, mainly in the field of 5G mm wave and automotive application.

Jaesik Kim

received B.S. and Ph.D. degrees in radio wave engineering from Kwangwoon University and electrical and electronic engineering from Yonsei University, Seoul, Korea in 2011 and 2017, respectively. He joined Agency for Defense Development, Daejeon, Korea in 2017, where he is currently a Senior Researcher. His current research interests include direction-finding antennas and phases array antennas.

Jaehoon Choi

received the B.S. degree from Hanyang University, Korea in 1980 and the M.S. and Ph.D. degrees from Ohio State University, Ohio, USA in 1986, and 1989, respectively. From 1989 to 1991, he was a research analyst with the Telecommunication Research Center at Arizona State University, Tempe, Arizona. He had worked for Korea Telecom as a team leader of the Satellite Communication Division from 1991 to 1995. Since 1995, he has been a professor in the Department of Electronics and Computer Engineering at Hanyang University, Korea. He has published more than 290 refereed journal articles and numerous conference proceedings. He also holds over 90 patents. His research interests include antenna, microwave circuit design, and EMC. Currently, his research is mainly focused on the design of a compact multiband antenna for mobile wireless communication and antennas for biomedical applications.